Chapter 2

Theoretical and Experimental Characterization of Silicon Nanoclusters Embedded in Silicon-Rich Oxide Films

Néstor David Espinosa Torres,
José Álvaro David Hernández de la Luz and
Javier Martínez Juárez

Additional information is available at the end of the chapter

http://dx.doi.org/10.5772/67614

Abstract

We present theoretical calculations using DFT method and the Global Reaction Model (GRM) for molecular structures and photoluminescence (PL) and Fourier Transform Infrared (FTIR) spectroscopy for silicon nanoclusters (Si-NCs) embedded in silicon rich oxide (SRO) films. Correlations between theoretical predictions and experimental results are made taking as reference experimental results obtained from measurements performed on SRO thin films obtained by the Hot Filament Chemical Vapor Deposition (HFCVD) technique. Our theoretical predictions are general since they do not depend on the particular technique used to obtain such films but rather the suggested SinOn structures. A good correlation exists for Eg values for films grown at 1300°C corresponding to Si_8O_8 and $Si_{16}O_{16}$ molecular structures suggested and for films grown at 1150°C with Si_9O_9. Regards PL correlation, a film grown at 900°C gives a spectrum peaked at 440nm and 548nm while theoretical one shows peaks at 471nm and 549.8 nm for a structure $Si_{16}O_{16}$. Such sample with a further annealing displays peaks at 405nm, 749nm and 820nm with theoretical predictions at 415nm using Si_6O_6. As for FTIR, theoretical calculations predict vibrational mode frequencies of bonds Si-O and Si-H whose values are well located in the experimental frequency range corresponding to the structure $Si_{16}O_{16}$.

Keywords: silicon-rich oxide, luminescence, DFT, GRM

1. Introduction

It is well known that the crystalline silicon has no photoluminescence due to multiple phenomena of non-radiative recombination between electrons and holes, and that the SiO_2 presents photoluminescence both by its amorphous nature and by their large gap. The latter has been taken as a starting point to consider silicon-confined systems of great interest because they offer the possibility of light emission from silicon-based materials. Following the initial report of the light emission from porous silicon, announced by Canham, this has been a novel subject of intense scientific activity currently along with other confined systems. Particularly, from the latter, it results in emphasizing the importance of the silicon rich oxides thin films. The physical microscopic structure of SiO_x is still a subject of discussion nowadays, where its structural arrangement is a key knowledge to get a deep understanding of radiative emission mechanisms in this kind of nanostructured materials.

The silicon rich oxide (SRO) is a silicon oxide with silicon excess or at amount of oxygen less than that of a silicon dioxide (SiO_2), so that the best appropriate notation would be SiO_x, with $x = 0,\ldots,2$. This material, after heat treatment, has a phase separation being composed of silicon nanocrystals (Si-NCs) surrounded by silicon oxide (Si-NCs/(SiO_x), regardless of the technique employed to obtain them (for instance, LPCVD, PECVD, etc.) [1]. The density and size of the Si-NCs have a strong dependence on the annealing temperature, the concentration of silicon, the characteristics of the silicon substrate, the partial pressure ratios between the reactant gases, the used production technique and the surrounding atmosphere during the annealing. It is remarkable to point out that the presence of phase separation (Si-NCs/(SiO_x), with a fixed value of x, can produce Si-NCs embedded in SiO_x with different values of x respect to SiO_2 and, consequently, multiple defects appeared at the borders of the Si-NCs and also within them and probably porous silicon may be present there. The defects generated during the production of the material disappear with the annealing process, particularly, at temperatures greater than 1000°C. It has been reported that for annealing temperatures less than 1100°C, the generation of amorphous silicon clusters is favoured [2], while for higher temperatures, the number of interfacial states is increased between Si-NCs and SiO_x, therefore the number of defects is also increased. A great field of active investigation has been opened in order to understand the underlying physical mechanisms of the SRO, which give rise to its crystalline structure and optical properties because it is a material, which promises important applications mostly in optoelectronic devices.

In the study of the SRO, one branch of research is focused on investigating the main mechanisms, which generate the luminescence phenomena in this material. In the case of structures such as SRO thin films, we found in the literature different approaches. So, it has been proposed several mechanisms involved in the luminescent emission observed, these include among others: quantum confinement of excitons, luminescence due to chemical species (such as siloxanes, silicon oxides and sub-oxides), interfacial states, defects and strain-related luminescence. Although there is a growing consensus that the quantum confinement effects (QCE) may explain some of the features of the two luminescence spectra [3], it is clear that in some cases, at least, other mechanisms are present. Up to now, there are no models that include several of these emission mechanisms.

In the proposal of quantum confinement as the dominant mechanism in luminescent effect, Qin and Li [4] proposed a limit on the size of the Si-NCs, considered as a critical size, above which dominates the quantum confinement effect while below it the effect of interfacial states prevails above all. With respect to photoluminescence in SRO including Si-NCs, it has been reported that it is dominated by strong quantum confinement above from a critical size of Si-NCs which may be about 1.1 nm in diameter, it corresponds to 10 times the Bohr radius of silicon, below this critical size, the photoluminescence may be dominated by the weak quantum well confinement as the interfacial defects.

Moreover, luminescent phenomenon in SRO structures can be excited by different forms, so we find that experimentally, luminescence spectra are generated by photoluminescence (PL), electroluminescence (EL) and cathode luminescence (CL) mechanisms. The fundamental physical mechanisms, which explain correctly the origin of luminescent phenomena in each one of these different forms of excitation, are still an active field of research.

Today, a few models are frequently used to describe a SRO network, namely the Mixture Model (MM) by Bell and Ley [5], the Random Bonding Model (RBM) by Philipp [6], and the Intermediate Model (IM) introduced in 2011 by Novikov and Gritsenko [7]. In 2012, Davor et al. [8], in an extensive review, considered that the actual structure seems to be greatly determined by the deposition procedure. In some works, the SiO_X structures films obtained by radio-frequency sputtering and physical evaporation were claimed to correspond to RBM, whereas the SiO_x films obtained by magneto-sputtering, Plasma-Enhanced Chemical Vapor Deposition (PECVD), have been assigned to MM. IM was used to describe SiO_x layers prepared by low pressure chemical vapour deposition (LPCVD) technique using SiH_4 and N_2O as a reactant precursors at 750°C. Finally, we find a new model, the Global Reaction Model (GRM) suggested lately by Espinosa-Torres et al. [9]. This model describes, first, the global and partial reaction(s) compulsory to produce the oxide matrices (SiO_2, Si_2O_3, SiO and Si_2O), second, the annealing reactions for elucidating the compositional changes after and before the thermal treatment, and subsequently, the variations in the intensity of luminescence spectra, and also it describes a set of secondary reactions of the oxide matrices with the hydrogen produced in the reaction chamber to obtain the charged species that could be associated to the emission in SRO thin films with explicit defects. This work is focused on studying the theoretical predictions about PL luminescence of SRO thin films based on DFT method and the GRM and make correlations with experimental PL results provided by measurements from SRO thin films obtained experimentally by the hot filament chemical vapour deposition (HFCVD) technique.

2. Relevant characteristics of silicon-rich oxide (SRO)

2.1. Some techniques of production of SRO

Among the different techniques used for depositing thin films, we can mention those which are commonly employed to grow SRO as a nanostructured material. One such technique is called hot filament chemical vapour deposition (HFCVD). This technique is known by different names like initiated-CVD (I-CVD), catalytic-CVD (Cat-CVD) and hot wire-CVD

(HWCVD). Amorphous and micro-crystalline silicon could also be obtained with this method [10]. The HFCVD technique gives some important advantages, it does not need a sophisticate temperature control and vacuum system, in addition, the deposition is free of plasma and we can obtain the precursors by a solid source or mixtures of gases. HFCVD system utilizes quartz-like solid source and makes use of the collision theory in order to describe the SRO deposition process [11]. The solid source to obtain SRO is made of Quartz, and it is etched by H^0.

Another technique is that known as low pressure chemical vapour deposition (LPCVD), it allows us to get silicon-rich oxide layers using oxide species like nitrous oxide (N_2O) and silicon compounds (silane, SiH_4) as reactants gasses. Silicon excess is easily controlled by changing the partial pressure ratio R_o between N_2O and SiH_4 defined by $R_o = P(N_2O)/P(SiH_4)$ or simply $R_o = N_2O/SiH_4$.

When we make a SRO layer, first, the partial pressures must be calculated by choosing a suitable R_o and P_T value. The suitable pressure for each reactant gas is calculated by means of relations,

$$P_{SiH_4} = \frac{P_T}{\frac{R_o}{20}+1} \; ; \; P_{N_2O} = \frac{R_o P_{SiH_4}}{20} \tag{1}$$

where P_{SiH_4} is the partial pressure of diluted silane at 5% (by this reason, term 20 appears) in nitrogen, P_{N_2O} is the nitrous oxide partial pressure and P is the total pressure. Si excess in the deposited films is controlled by the partial pressure ratio R_o of the reactants gases.

The optical characteristics of SRO, obtained by this technique, can be varied with the excess silicon in the films, making SRO attractive to fabricate optoelectronic devices. Therefore, Si-NCs embedded in a SiO_2 matrix are currently attracting much interest to be a good candidate for building efficient light-emitter devices [12–14]. Such devices are highly desirable for the integration of optical signal and electronic data processing circuits on the same chip. Furthermore, its fabrication process is compatible with the present large-scale integration technologies [15, 16]. The native band gap of Si-NCs is enlarged with respect to one of the bulk material; this fact brings the possibility to observe an intense visible PL spectrum at room temperature. The PL spectrum consists generally of intense emission peaks in the near-infrared (NIR) and visible (VIS) regions. It was established that blue and green PLs are caused by various emitting centres in the silicon oxide, while the nature of the intense PL in orange-red region is still discussed [17–19].

Experimentalists have reported in the literature that emission spectra of the SRO films vary in the interval of wavelengths from 400 to 850 nm for layers deposited by LPCVD. It has not been observed experimental emission outside of this range for samples obtained by this technique. Nevertheless, by preliminary theoretical studies, using the density functional theory (DFT), it has been found as isolated molecules, presumably found in SRO thin films that could emit in UV region.

In addition, for SRO thin films deposited by LPCVD, PL is only observed in annealed samples. In fact, only thin films annealed at 1100°C produce high emission, and the highest photoemission is obtained for SRO films with $R_o = 30$, which corresponds to a silicon excess about 3%,

and R_o = 10 corresponds with a silicon excess about 12%. The PL is only obtained from the visible (VIS) to NIR range, and its intensity reduces as R_o decreases. In contrast, we find that powders and thin films SRO deposited by other technique such as HFCVD technique, display a reduction in photoluminescence intensity in most cases after being annealed, and only in very particular conditions (deposited parameters) the PL is increased.

By using the LPCVD technique, the SRO refractive index can be changed, it has been reported that the index varies from 1.45 to 1.94 when the silicon excess is changed. It is observed that the refractive index of the SRO on silicon substrate increases with the increment of Si excess, it means that as R_o augments, the index tends towards the refractive one of SiO_2, contrarily, it tends towards that of Si. Then, by measuring the refractive index, the inclusion of Si in these SRO films is easy to detect. For example, it has been found that for R_o = 10, after thermal annealing, the refractive index reaches values greater than 2. In contrast, when the reactant ratios are R_o = 20, 30 and 40, the refractive indexes diminish with a clear tendency to reach values less than 1.5 [20].

Relating to transmittance of SRO obtained by LPCVD (an important optical parameter measured in experiments), we find that the transmittance spectra for R_o = 10, 20, 30 films deposited on sapphire substrates are reported in Ref. [2]. According to this reference, the observed transmittance of these films deposited on sapphire is high (>80%) and vanishes to zero when wavelength reduces. The annealing time parameter does not produce a clear variation on transmittance; however, when R_o parameter undergoes increments it causes a clear shift of the curves towards lower wavelength. The absorption coefficients are determined from transmission spectra, and it can be observed that the position of the absorption edge moves towards higher energy when R_o increases.

Other important technique is the sputtering one, where sputtering means an ionic bombardment process in vapour phase at room temperature. By this technique, plasma is formed by the ionized process gas, usually Argon, due to the presence of a strong electric field. The high voltage between cathode and anode causes that ions of the process gas hit the target with enough energy to pull out atoms from the surface of the target (cathode) by a momentum transfer process. The multiple collisions enable some atoms of the material acquire enough energy to leave the surface, then reach the substrate and stick to it. Sputtering technique can be divided into reactive and non-reactive. It is denominated no reactive sputtering to one in which the process gas does not react with the deposited material. Typically, Argon is used as inert gas due to the high yield obtained and its minor cost. When sputtering is made in the presence of a reactive gas as oxygen, the sputtering is called reactive. In this case, the presence of ionized oxygen causes oxidation of the material, thus obtaining films whose properties depend on the concentration of reactive gas in the chamber during the process.

In the sputtering technique, the growth model of SRO films is based in the work proposed by Nyberg and Berg [21], where they describe the reactive sputtering processing behaviour in many different ways to carry out. This model has been specially adapted to the growth of SiO_x films where the growth kinetics is dependent on the flux of oxygen onto the substrate surface relative to the flux of Si incorporated into the film.

As to the optical properties of the Si/SO_x, they differ due to the synthesis technique, indicating structural differences of the Si-NCs (as silicon nanocrystals, amorphous silicon and defects) and their environment [22]. Raman scattering measurements are frequently used to prove the presence of Si-NCs. With this fast and non-destructive method, it is possible to determine whether silicon particles are amorphous or crystalline. Moreover, information about mean size (MS) and sizes distribution (SD) of nanocrystallites can be obtained from the peak position and shape of the Raman band. For samples using Si wafers as substrates, Raman measurements must be undertaken with care because the strong Raman peak from the crystalline Si (c-Si) substrate masks the signal of the Si-NCs. To avoid this problem, sapphire substrates should be used. Then, the obtained Raman data can clearly be related to the deposited thin film, not to the substrate.

2.2. Morphological aspects of SRO films

Figure 1(a) shows SEM micrograph of SRO film deposited by HFCVD at 409°C. The characteristics of the films depend on the deposition conditions such as substrate temperature, deposition time, solid sources and kind of substrate. So there are several factors that can change the morphology of the films. In this figure, we can see agglomerate structures, which form isomers Si_7 with sphere shape; this geometric shape is a consequence of the elevated temperature. Also, we can appreciate that there are interspaces among agglomerates, so it leads to the formation of a porous film.

On the other hand, silicon-rich oxide powders (SROP) agglomerates and frost can be seen more clearly in SEM Micrographs shown in **Figure 1(b)** and **(c)**, where we can see that the big silicon rich oxide powders (SROPs) are formed by the agglomeration of small nanoparticles. The excess of precursors in gas phase is called supersaturation, and it is present in all SROP samples. In HFCVD technique, the filament-source distance controls the supersaturation. Therefore, the morphology is controlled by the saturation and growth temperature. This process can be described in the following manner: the precursor reacts in gas phase, and it creates clusters in the environment. Some clusters could be composed by silicon, silicon-hydrogen, silicon monoxide and silica as powder. The temperature between filament and source is very high, but it decreases between source and substrate due to a temperature gradient within the filament. When the distance of source-substrate increases, the growth temperature decreases, and with this conditions, the environment is supersaturated and it is partially condensed.

Relevant differences in SEM images shown in **Figure 1(a)–(c)**, are originated owing to the deposition temperatures, which were 409, 368 and 320°C, respectively. Grains formed at the highest temperature are bigger due to the matrix SiO_2 that embedded silicon agglomerates or nanocrystals. Presence of silicon agglomerates was corroborated using micro Raman. Images of **Figure 1(a)** and **(b)** were taken with the secondary electron detector for high-resolution images. This detector uses a lower voltage, which favours the superficial resolution of images. In **Figure 1(b)** is observed a porous surface, probably formed by smaller isomers than those formed at 409°C, where their size is considerably greater than 8 μm.

Finally, **Figure 2** displays results of band gap values obtained by applying the Kubelka-Munk method to SiO_x powders deposited by HFCVD at the temperatures of 300, 320 and 539°C and filament-source distances of 2, 9 and 10 mm whose values are 3.42, 3.63 and 3.72 eV, respectively [23].

http://dx.doi.org/10.5772/67614

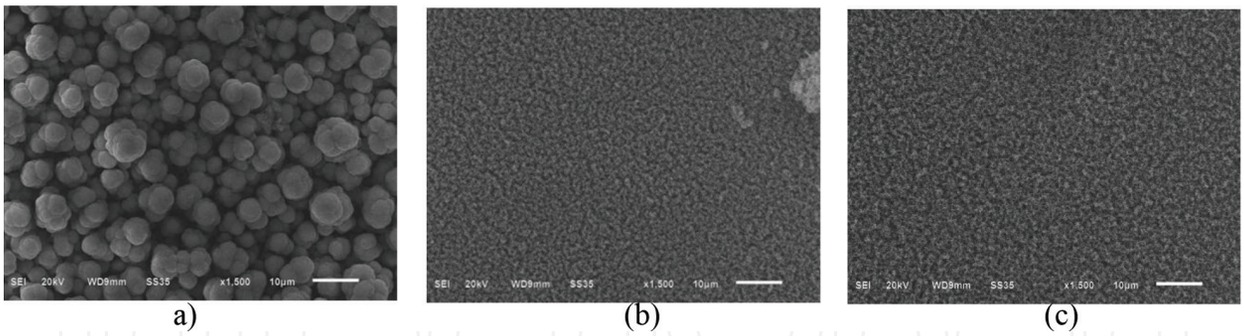

Figure 1. SEM micrograph of a SRO film deposited by HFCVD (a) at 409°C, (b) at 368°C and (c) at 320°C.

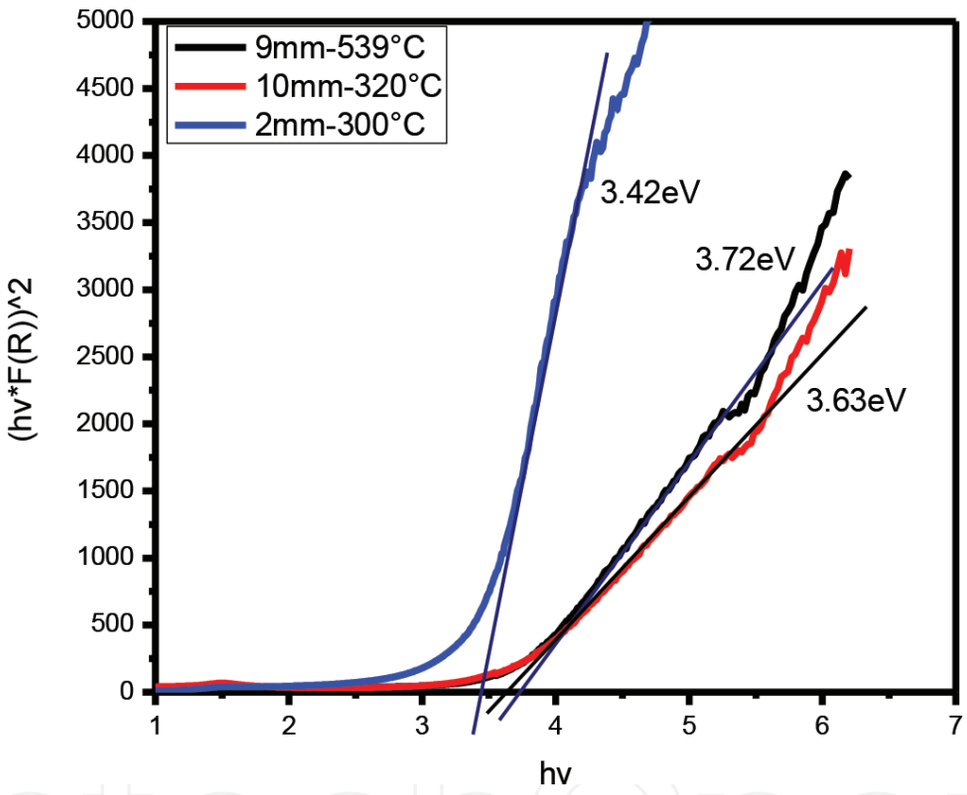

Figure 2. Band Gap values of SRO films measured by Kubelka–Munk's method.

3. Correlation between experimental results and theoretical predictions of the Global Reaction Model (GRM)

3.1. Global Reaction Model

In this section, we present for first time a new model, which considers the global and partial reaction(s) necessary to generate the oxide matrices (SiO_2, Si_2O_3, SiO and Si_2O), the annealing reactions for explaining the compositional changes after and before the thermal treatment and consequently the changes in luminescence spectra intensity and a set of secondary reactions of the oxide matrices with the hydrogen produced to obtain the ions that could be

associated to the emission in SRO thin films with specific defects. When SRO is prepared by LPCVD, a gas mixture of N_2O and silane is habitually used [24, 25] and the excess Si content can be modified by the gas flow ratio $R_o = \left[\frac{N_2O}{SiH_4}\right]$. The silicon excess can be as high as 17% for $R_o = 3$; and experimentally stoichiometric SiO_2 (a non-free silicon film) can be obtained for $R_o \geq 50$ [26]. Theoretically, $R_o = 40$ corresponds to the stoichiometric silica, when a mixture silane-nitrogen at 5% is used. Experimentally, there is enough evidence that SRO thin films are constituted by a silicon oxides mixture and not only by one of them, independently of the value of R_o. We can establish the global reactions of the chemical combination of N_2O, N_2 and SiH_4, which generates the theoretical composition of SRO given by

$$SiO_2 = \frac{(1-x)}{(4+z+v)} \; ; \; Si_2O_3 = \frac{(1-v)}{4+z+v} \; ; \; SiO = \frac{(1-y)}{(4+z+v)} \tag{2}$$

$$Si_2O = \frac{(1-z)}{(4+z+v)} \; ; \; Si = \frac{(x+y+2z+2v)}{(4+z+v)} \tag{3}$$

where the parameters x, y, z, v satisfy the conditions $0 \leq x, y, z, v \leq 1.0$ and $0 \leq x+y+2x+v \leq 1.0$.

When SRO thin films are annealed, some oxides are degraded. The plausible 'annealing reactions' proposed are as follows:

$$SiO_{2(solid)} + \text{Heat} \rightleftarrows (1-\xi)SiO_{(solid)} + (0.5+0.5\xi)O_{2(gas)} + \xi\, Si_{solid} \tag{4}$$

$$Si_2O_{3(solid)} + \text{Heat} \rightleftarrows (1-\xi')Si_2O_{(solid)} + (2+\xi')O_{2(gas)} + 2\,\xi'\, Si_{solid} \tag{5}$$

Double arrow stands for denoting equilibrium condition, ξ *and* ξ' are the progress of the annealing reactions. The extent of progress of reaction is defined as the ratio between the total change in the number of moles of a species and their stoichiometric coefficients.

As is known, a mole of any substance contains the number of atoms equal to the Avogadro's number, $N_A = 6.023 \times 10^{23}$. In order to perform first-principles calculations, the problem must be modelled with a maximum of 100 atoms, consequently, the oxides must be rewritten in terms of the number of atoms, that is, Si_nO_{2n}, $Si_{2n}O_{3n}$, Si_nO_n and $Si_{2n}O_n$. The hydrogen gases can react accordingly as $H_2 = [H]^+ + [H]^-$.

The hydrogen ion formed, in turn, reacts with the silicon oxides to form ions such as $\left[Si_nO_{2n}H\right]^+$, $\left[Si_nO_{2n}H\right]^{2+}$ etc. During heat treatment the reactions produce a dehydration of these cations, resulting in the formation of new ones, for example, $\left[Si_nO_{2n}H_2\right]^{2+} \Leftrightarrow \left[Si_nO_{2n-1}\right]^{2+} + H_2O\uparrow$, and so on. Finally, the moieties obtained from these reactions result as follows:

$$\left[Si_nO_{2n-1}\right]^{2+} \; ; \; \left[Si_{2n}O_{3n-1}\right]^{2+} \; ; \; \left[Si_nO_{n-1}\right]^{2+} \text{ and } \left[Si_{2n}O_{n-1}\right]^{2+}. \tag{6}$$

These anions formed are different oxides matrices containing vacancies or defects of silicon which may or not be present in the films of SRO.

3.2. Comparison between experimental results and theoretical predictions of GRM.

In this section, we will display and discuss the results employing DFT to evaluate theoretically structures type Si_nO_n, where $5 \leq n \leq 26$ is the number of silicon atoms. The GRM already discussed is employed to explain the physical microscopic structure of SRO thin films regardless

http://dx.doi.org/10.5772/67614

of the technique used to obtain the SRO structure since we are only interested in its molecular composition and atomic arrangement. Also, we will show the results of the evaluation of structural and optical properties for a wide set of moieties, seemingly found in SRO. DFT results predict emission in visible region for molecules with a number of atoms less than 14 silicon ones. Results obtained in this research predict luminescence in visible region for just about half calculated structures, especially for $n \leq 16$ silicon atoms, while large structures with $n \geq 17$ display luminescence in ultraviolet region.

3.3. Measurements of band gap E_g for SiO_x thin films

We begin by taking SiO_x films obtained by HFCVD technique from our experimental group (results not even published). From these samples, we take into account the band gap parameter as the first one to be analysed. The approximate experimental values of the energy band gap E_g are obtained by the relationship known as Tauc plot [27] as shown in **Figure 3(a)**. The methodology for obtaining the E_g has been described in a previous work [28]. It is found that E_g decreases when the substrate temperature is raised. The band gap of the SiO_x films lies in the range of 1.8–2.5 eV. When x decreases out from 2.0 in a $—SiO_x$ (amorphous oxide), the valence band edge moves up, as the increased Si—Si bond states are gradually overlapped with the oxygen non-bonding states (ONS), and finally spread out into the Si valence band. Simultaneously, the conduction band edge also moves down, giving rise to the band gap decreasing nonlinearly when the Si concentration is increased continually.

In **Figure 3(a)**, we observe that by making an extrapolation through the straight line according to Tauc procedure, we obtain the approximated bang gaps which have values of 1.95eV and 2.15 eV for **Figure 3(b)**. At first glance, the variations of E_g are originated by the difference in temperatures then it is observed that E_g reduces as temperature increases. These two experimental values of E_g fit well with those obtained theoretically using DFT as shown in **Table 1** further below that are results for structures type Si_nO_n.

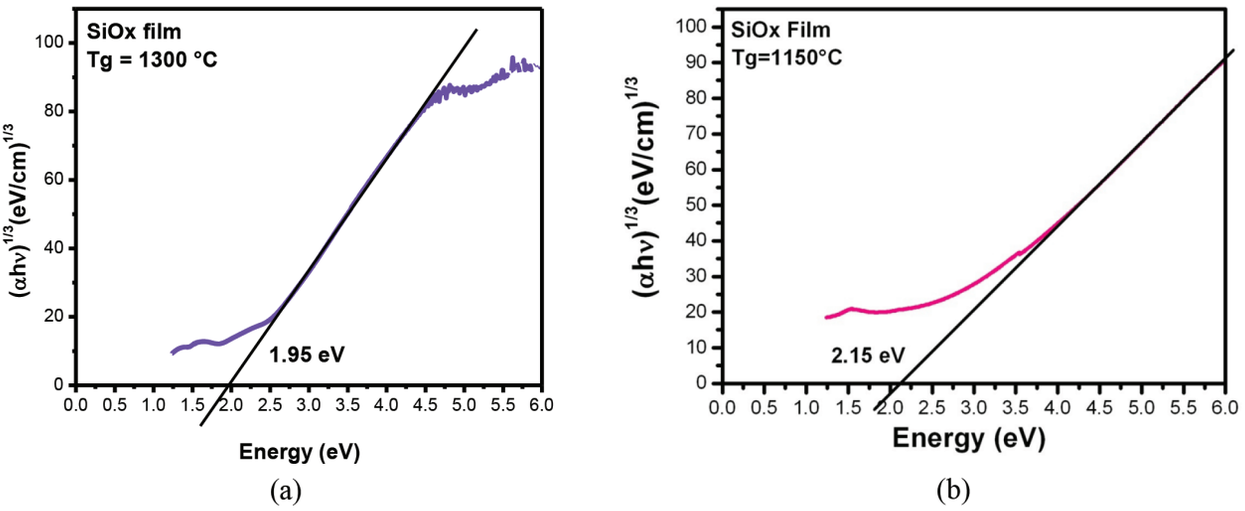

Figure 3. Determination of E_g for a SiO_x film by making use of the relationship known as Tauc plot $[\alpha(h\nu)]^{1/3}$ versus energy ($h\nu$) for two temperatures (a) T_g =1300°C and (b) T_g =1150°C.

Number of silicon atoms	HOMO eV	LUMO eV	GAP eV
5	–6.19	–3.14	3.05
6	–6.01	–3.46	2.55
8	–5.51	–3.58	1.93
9	–5.34	–3.28	2.06
11	–5.93	–3.22	2.71
12	–5.97	–2.96	3.01
13	–5.61	–3.30	2.31
14	–6.04	–2.79	3.25
15	–6.11	–3.39	2.72
16	–6.16	–4.20	1.96

Table 1. Highest Occupied Molecular Orbital (HOMO), *Lowest Unoccupied Molecular Orbital* (LUMO) and HOMO–LUMO gap calculated using DFT for $[Si_nO_n]$ structures with $5 \leq n \leq 16$.

We have seen that SiO_x thin films, deposited at T_g = 1300°C, resulted with a bang gap of 1.95 eV, calculated using Tauc technique.

Now, by observing **Table 1**, we can correlate two possible theoretical values either E_g = 1.93 eV corresponding to Si_8O_8 molecule or E_g = 1.96 eV corresponding to $Si_{16}O_{16}$ one, existing the possibility of a mixture of them. On the other hand, SiO_X film deposited at 1150°C corresponds to an approximated experimental band gap of 2.15 eV, which correlates well with a theoretical value of E_g = 2.06 eV associated to Si_9O_9 molecule in accordance with **Table 1**.

In regard to the origin of the PL emission in Si-NCs, it is still a subject of debate; however, we can find some proposals of models suggested explaining this phenomenon. One of this model relates the PL to quantum confinement effects (QCEs) [29, 30]. The other model relates the PL to defects in the oxide matrix or at the interface SiO_2/Si-NCs [28, 31].

Broadly, both common accepted proposals make use of approximated quantum methods in order to solve the Schrödinger equation associated with quantum confinement of the electron restricted to move in so small spatial dimensions, thence their predictions about luminescent phenomenon are limited. Considering this important fact, we hope that an analysis of this phenomenon made from the view point of composition and molecular structures can significantly contribute to a better knowledge of luminesce in SRO considered as an arrangement of Si-NCs embedded in oxide matrices.

3.4. Thermal effects in PL of the SiO_x thin films

Now, we proceed to our analysis in relationship to PL phenomenon. Inspecting, in **Figure 4(a)**, the experimental PL spectrum measured from the SiO_x film as grown at T_g = 900°C, we locate two emission bands both covering a wide spectral range from 380 to 750 nm (from violet to red).

http://dx.doi.org/10.5772/67614

The left band peaked around 440 nm while the right one peaked around 548 nm as can be confirmed by de-convolution curves. After making a further annealing to the same SiO_x film, the PL spectrum **Figure 5(a)** displays two main bands, one is the A band, which lies in the violet-blue range (380–495 nm) peaked at 405 nm with a relatively weak PL intensity. The other band is the B one, which lies in the orange-near infrared range (590–875 nm), this band shows a strong intensity and two main peaks, one located at 749 nm and other at 820 nm as confirmed again by de-convolution curves.

Looking at **Figures 4(a)** and **5(a)** and making comparisons between them, we infer that the PL intensity that decreases after thermal annealing [32] due to the PL intensity is lower after a further annealing. According to this result, we conclude that annealing process stimulates the formation of crystalline silicon (c-Si) as well as the formation of defects both contributing to the PL emission. For this reason the PL spectrum shifts to the red region.

With regard to the theoretical PL spectrum, **Figure 4(b)** exhibits this one, for the SiO_X film as grown at T_g = 900°C, that was calculated considering the arrangement of a $Si_{16}O_{16}$ molecule. With this molecular structure, we obtained the PL spectrum which has two remarkable peaks, one of them located at 471 nm with the highest intensity and the other has two located peaks closer at 549.8 and 556 nm. In addition, an excited state at 683 nm was also found, but its intensity was too negligible or non-detectable.

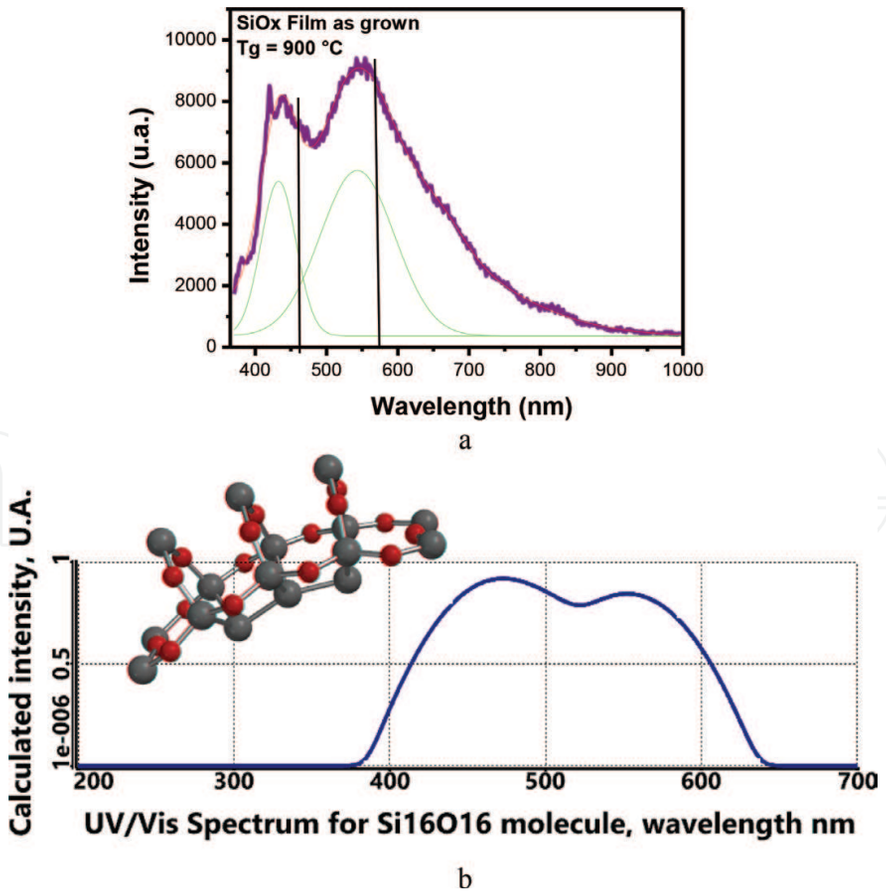

Figure 4. (a) Experimental PL spectrum from a SiO_x film grown at 900°C. (b) Theoretical PL spectrum calculated for $Si_{16}O_{16}$ structure.

To complement the study of the PL spectrum including annealing effects, in **Figure 5(b)** we display results for the theoretical PL spectrum calculated by considering a small molecule type Si_6O_6. With this molecular structure we predicted excited states emitting in the region from 393.78 to 415.59 nm in addition to a region peaked at 772.8 nm, which corresponds approximately to the left side of the wide shoulder observed in the experimental spectrum displayed in **Figure 8** where the de-convolution curve points out a peak at 749 nm. We emphasize that in this theoretical spectrum the presence of the peak at 820 nm found in the experimental PL spectrum is not clear.

In relation to the study of the configuration of the molecular structure, we present in **Figure 6(a)** the two structures corresponding to the case of the SiO_x film as grown at T_g = 900°C and after a further annealing **Figure 6(b)**, both structures correspond to

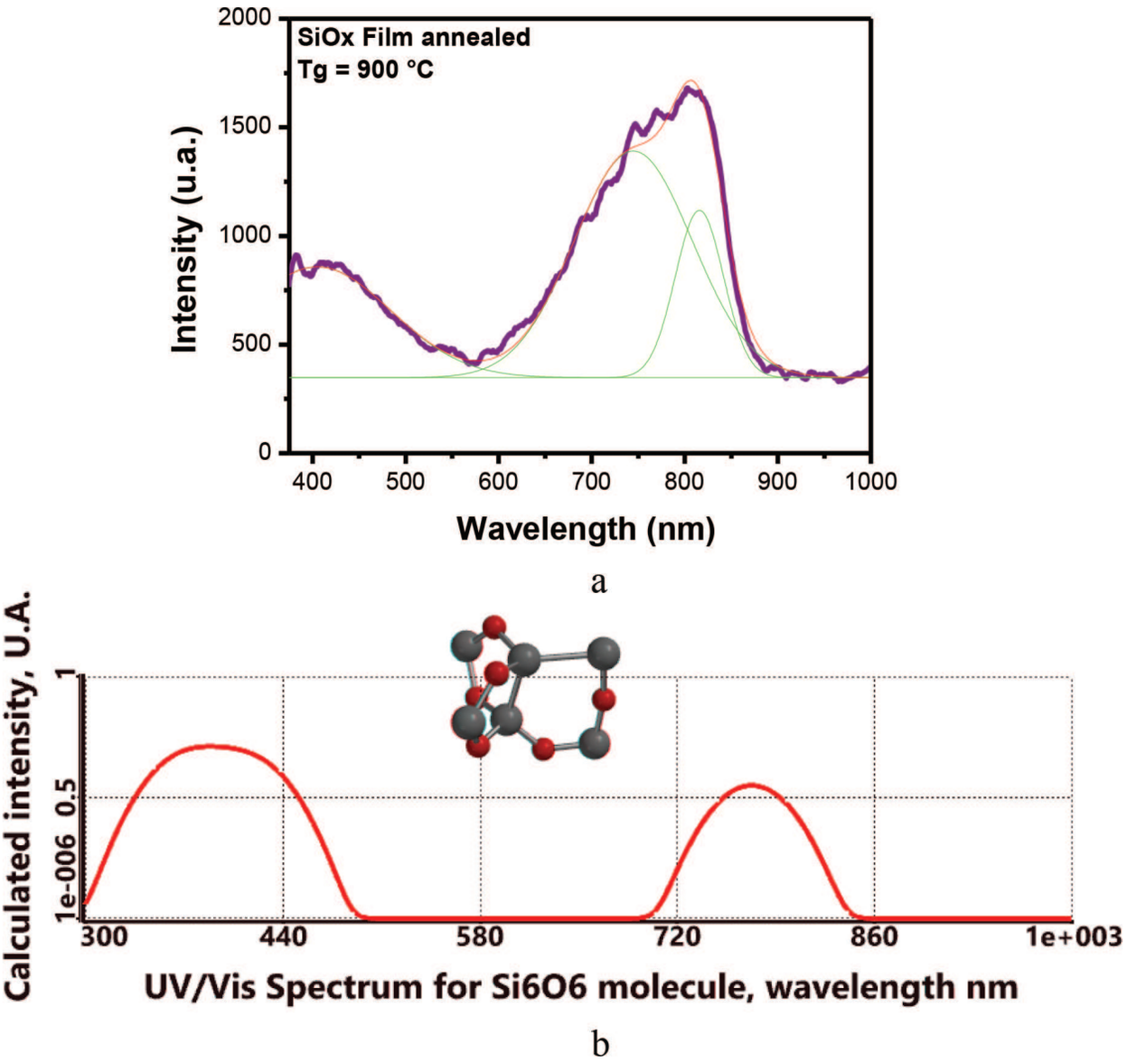

Figure 5. (a) Experimental PL spectrum from a SiO_x film after a further annealing. (b) Theoretical PL spectrum correlated to the experimental one of (a), including the annealing effects. This spectrum is reproduced by means of considering the small molecule type Si_6O_6.

http://dx.doi.org/10.5772/67614

$Si_{16}O_{16}$ molecule. The structure at the top of the figure consists of 16 hydrogen atoms linked to eight silicon atoms with tetra valences forming the $Si_{16}O_{16}$:H_{16} arrangement. On the other hand, in the bottom we display the $Si_{16}O_{16}$ molecule after annealing. It could be described as a set of seven rings constituted of three member's mini rings each one with two bonds Si—O and a third link Si—Si. There are four mini rings with a semi-circular arrangement and the rest is in orthogonal position.

Regarding the molecular structure proposed for molecule Si_6O_6:H_8 (as grown), it is represented at the top of **Figure 6(c)**, whereas at **Figure 6(d)** we localize the corresponding molecule Si_6O_6 after a further annealing. This molecule was proposed for modelling the SiO_x film after being annealed at 900°C. The structure of this molecule consists only of three mini-rings, two of which are three member rings with two Si—O bonds and one Si—Si bond. The third ring has four silicon atoms with two Si—O bonds and a Si—Si—Si chain. Within the molecule as grown, that is Si_6O_6:H_8, the six silicon atoms have tetra valence.

We now deal with the situation where the growth temperature of H_8SiO_x film is increased. This implies that the molecular structure should be modified giving rise to another new one with different properties. In **Figure 7(a)**, we display the experimental PL spectrum measured from a SiO_x film as grown at temperature of 1150°C.With the naked eye a wide band is identified at right hand and approximately half wide band at left side. Through de-convolution curves of this spectrum, we can locate the positions of maxima of both bands. The half wide band is peaked around 385 nm and the right band around 690 nm.

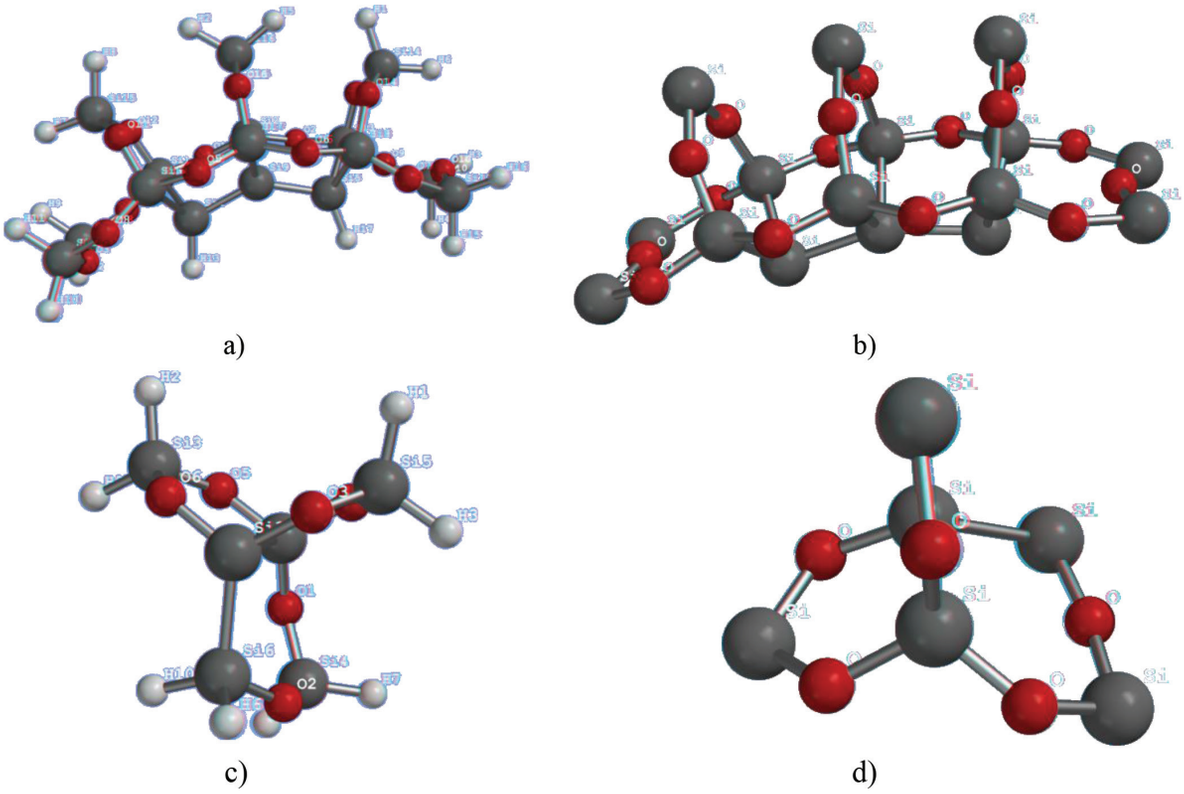

Figure 6. Molecular structure suggested for the SiO_x film: (a) $Si_{16}O_{16}$:H_{16}, as grown at T_g = 900°C (b) $Si_{16}O_{16}$ after a further annealing. Molecular structure proposed for modelling the SiO_x film after being annealed at 900°C, (c) as grown is type Si_6O_6:H_8 and (d) after annealed is type Si_6O_6.

Comparatively by **Figure 7(b)** we can observe the correlated theoretical PL spectrum calculated for $Si_{11}O_{11}$ molecule. With this molecular structure, we have predicted a PL spectrum having only two bands where the half left band possesses the highest intensity being peaked at 380 nm, and the other one with lower intensity and its maxima corresponds to an excited state of emission at 699 nm. In this case, we did not look for triplets for $Si_{11}O_{11}$ molecule, taking for granted that if they exist they would have a negligible intensity.

Furthermore, the molecular structure suggested for $Si_{11}O_{11}$ molecule is represented in **Figure 8(a)** that corresponds to as grown molecule $Si_{11}O_{11}:H_{12}$. In the arrangement of this structure we figure out that there are 12 hydrogen atoms joined to six silicon ones with tetra valence. The 'backbone of this molecule' is a silicon atom joined to four silicon atoms shaping a tetrahedral arrangement, with six mini rings constituted where five of them have four silicon atoms and two Si—O bonds each one and a Si—Si—Si chain. The sixth mini ring has only one Si—O bond and a large silicon chain Si—Si—Si—Si. **Figure 8(b)** represents the after-annealed condition for the molecular arrangement of $Si_{11}O_{11}$.

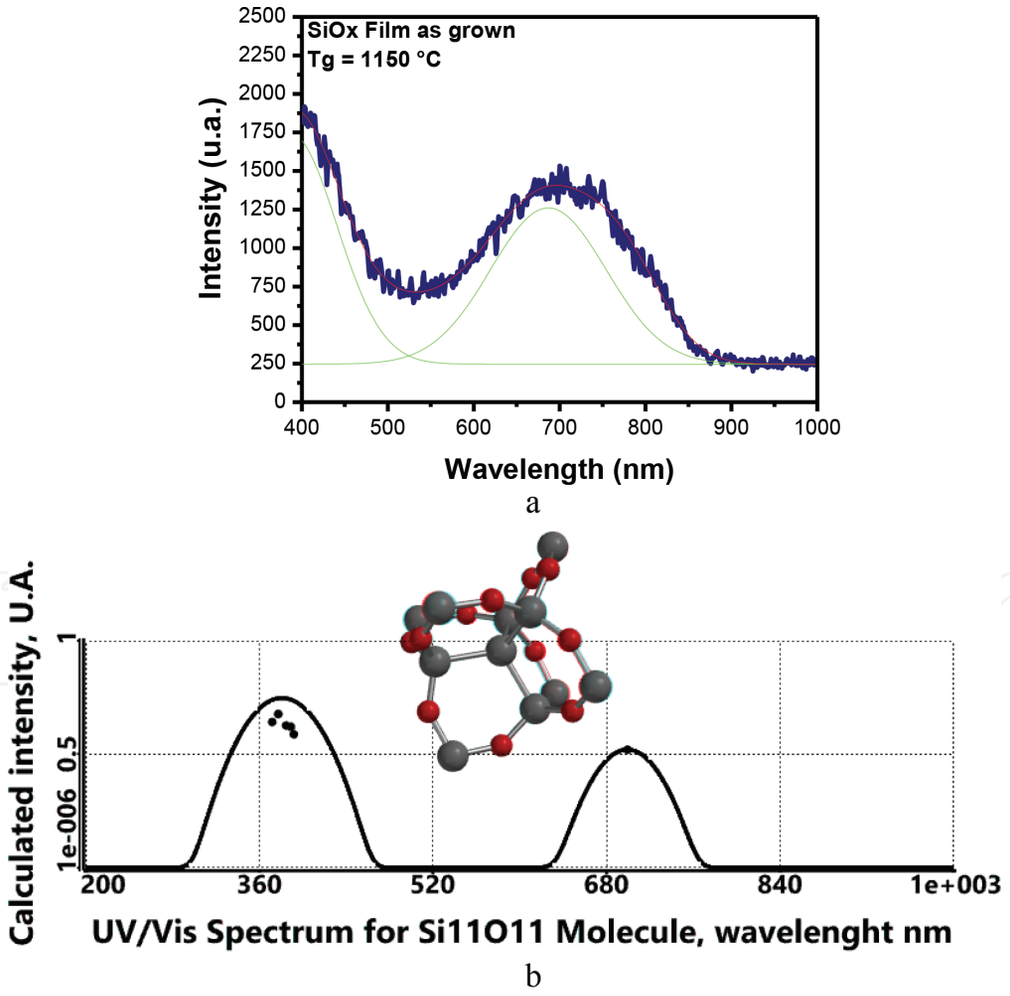

Figure 7. (a) Experimental PL spectrum of a SiO_x film as grown at 1150°C. (b) Correlated theoretical PL spectrum of (a). In this case the SiO_x film is modelled with a molecular structure of type $Si_{11}O_{11}$ molecule.

http://dx.doi.org/10.5772/67614

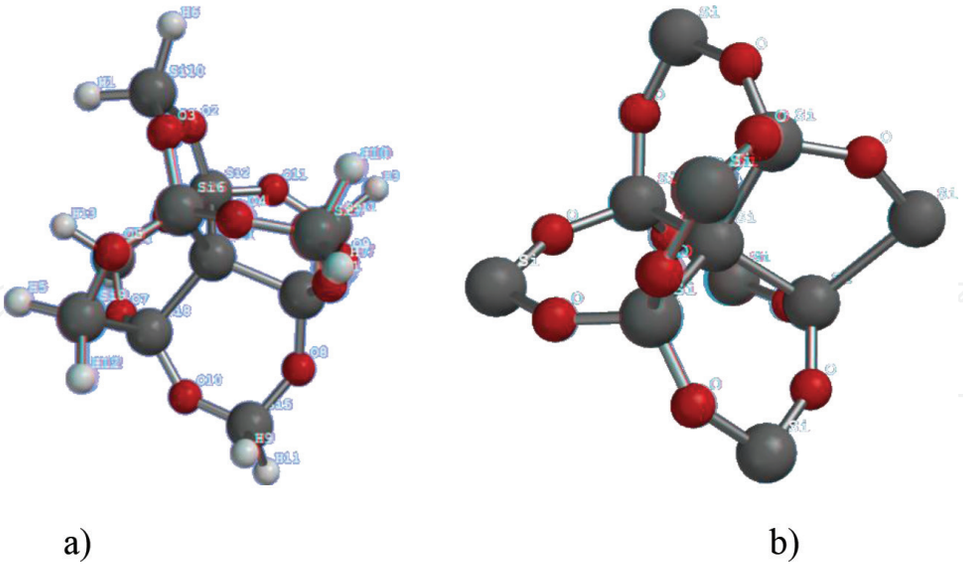

Figure 8. Molecular structure suggested. (a) As grown it corresponds to $Si_{11}O_{11}$:H_{12} arrangement, (b) after annealed, the molecular arrangement is type $Si_{11}O_{11}$.

3.5. FTIR spectra of the SiO_x thin films

In order to get a more complete evaluation of the optical and structural properties of SRO structures, we now proceed to make a theoretical analysis of Fourier Transform Infrared (FTIR) spectroscopy. In practice, FTIR is a technique used for structural characterization of materials with which it is possible to study atomic bonds between elements that are present in a given film. The various bonds are manifested as different absorption bands which lie in different wavelength ranges. The position and shape of these bands are related to the density, stoichiometry and the nature of the bond primarily. The infrared energy causes vibrational motion of atoms in a molecule identified as rocking, stretching, wagging and bending when they interact with such energy. A fraction of the incident radiation is absorbed at specific wavelengths. A molecule must vibrate so that there is a displacement from the electrical centre and absorbed radiation in the infrared region, that is, there must be a change in the dipole moment.

In **Figure 9(a)** we display the experimental FTIR spectrum of a SiO_x film as grown at 900°C. According to Ay and Aydinly [33] they have associated these vibrational frequencies as indicated in **Table 2**. In such **Table 2**, we make comparisons between vibrational frequencies as found experimentally in **Figure 9(a)** and theoretical frequencies as obtained in this report when considering a $Si_{16}O_{16}$ molecule in addition to being identified with the different vibrational modes reported in literature. Particularly, the experimental frequencies at 654 and 875 cm^{-1}, in **Figure 9(a)**, have been associated as reported in the literature to Si—H vibrational frequencies. Comparing these frequencies with those found by our theoretical calculations, we find discrepancies since we observed such frequencies at 652 and 885 cm^{-1} which are due to Si—Si and Si—O bonds.

Apart from discrepancies in their values between experimental and theoretical frequencies, we also find differences between their associated intensities as is evident from **Figure 9(a)**

when is compared with **Figure 9(b)**. Two very remarkable differences in their intensities are found in peaks located at 875 and 1051 cm^{-1} in the experimental FTIR spectrum and their correlated theoretical values located in **Figure 9(b)** approximately at 885 and 1058 cm^{-1}, in fact, if we observe carefully theoretical and experimental intensities are inverted in magnitude.

On the other hand, we stress that plot in **Figure 9(b)** corresponds to a Gaussian curve fitted to FWHH = 40, whereas plot in **Figure 9(c)** corresponds to a Gaussian curve fitted to FWHH = 80. We can observe clearly that the difference in Full Width at Half Maximum (FWHH) values gives rise to the effect that the peak at 1058 cm^{-1} in **Figure 9(b)** is transformed into a shoulder of the peak at 885 cm^{-1} as is shown in **Figure 9(c)**. The effect of varying FWHH to higher values causes the FTIR spectrum to become more intense in **Figure 9(c)**, it means physically the SiO_x film were thicker; in addition to this, FTIR spectrum resembles more to the experimental one of **Figure 9(a)** although discrepancies in wavenumbers continue to persist.

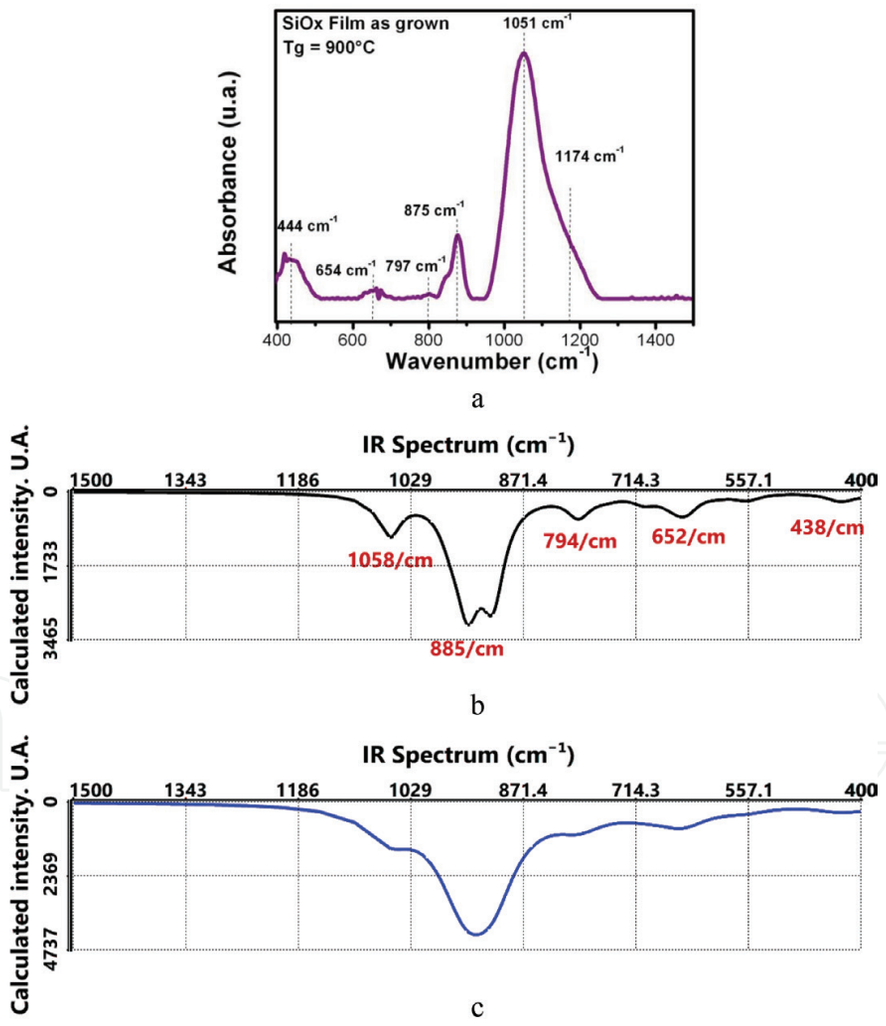

Figure 9. (a) Experimental FTIR spectrum from a SiO_x film as grown at 900°C, (b) theoretical FTIR spectra calculated using DFT for a $Si_{16}O_{16}$ molecule with FWHH = 40. Vibrational frequencies found in this spectrum when are correlated to those of (a) show discrepancies. This plot corresponds to a Gaussian curved fitted to FWHH = 40 and (c) same as (b) but FWHH = 80.

Now, we consider important to study the influence of annealing process on FTIR spectra. For this, we focus on a SiO_x thin film deposited at 900°C with a further annealing, normally carried out in the (1100–1150)°C range. **Figure 10** displays the experimental FTIR spectrum for this sample. It is worthwhile to mention that after the films have been heat-treated (annealed), the FTIR spectrum peaks corresponding or associated to Si–H vibrational frequencies disappear. Also, the uppermost peak which corresponds to Si–O stretching mode (1051 cm^{-1}) is considerably shifted to higher frequencies (1082 cm^{-1}) indicating a phase separation.

It is possible then, for example, that a molecule like $Si_{16}O_{16}$ can be transformed in a smaller molecule like $Si_{11}O_{11}$ or Si_6O_6 (it depends mainly on time and annealing temperature). On the other hand, it has been reported that amorphous silicon (a-Si) as well as crystalline one (c-Si)

	Wavenumber, cm^{-1}, SiO_x film as grown from 900 to 1150°C				
Associated in literature to	Si-O rocking	Si-H wagging	Si-O bending	Si-H bending	Si-O stretching
Experimental	429–444	645–654	797–810	875–885	1048–1064
Calculated using DFT		Si-Si bending in $Si_{16}O_{16}$ molecule		Si-O in 'external rings'	
Calculated	438	652	794	885	1058

Table 2. Comparison of vibrational frequencies observed experimentally in a SiO_x film as grown at 900°C versus calculated FTIR spectrum for a $Si_{16}O_{16}$ molecule.

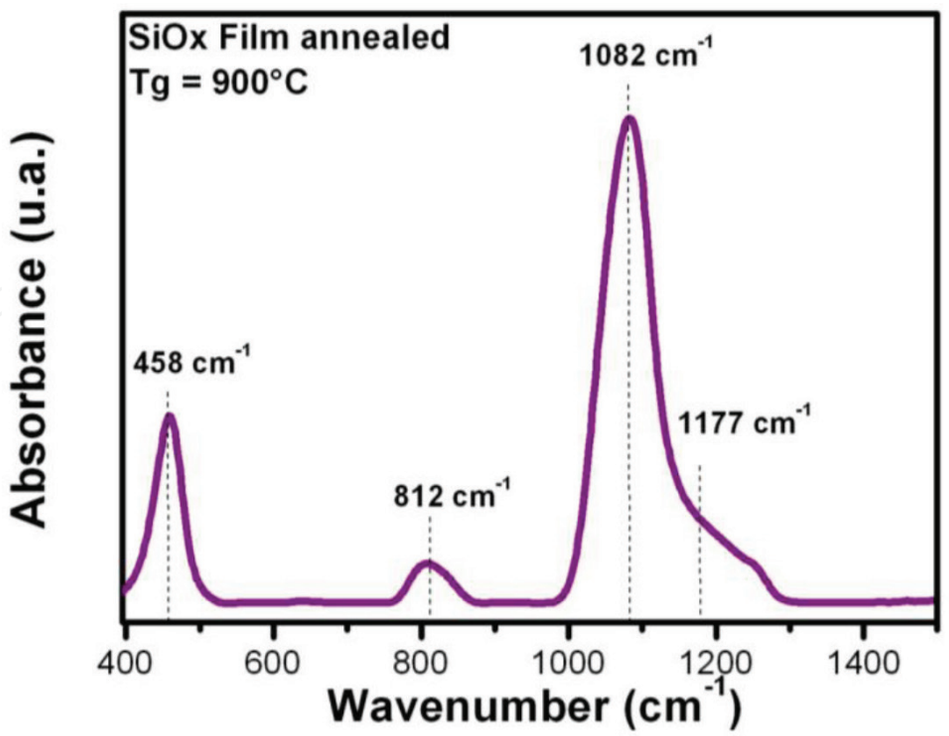

Figure 10. Experimental FTIR spectrum from a SiO_x thin film after further annealing.

could be identified by Raman spectroscopy [34]. A broadband around ~480 cm^{-1} is typically associated to a-Si, while bulk silicon has a sharp intensity peak around 521 cm^{-1}. As to Si-NCs, it is found that intensity peaks are shifted to smaller wavenumbers where this change is a function of decreasing Si-NCs size, this event has been extensively attributed to quantum confinement effects.

For example, in **Figure 11** which corresponds to a theoretical Raman spectrum that we have calculated for a $Si_{11}O_{11}$ molecule suggested, we can clearly identify frequencies at 460 and 508 cm^{-1}, respectively.

We have explained previously that the molecule $Si_{11}O_{11}$ has two chains, one is type Si—Si—Si and the other is a larger chain type Si—Si—Si—Si (tetragonal arrangement shape).

3.6. PL spectra of porous silicon in SiO_x thin films

Keeping in mind that in SRO thin films the generation of porous silicon as a consequence of phase separation of Si-NCs/SiO_x are present, as just mentioned in Section 1, its results are attractive as we apply our theoretical methods, used along the optical and structural analyses on SiO_x structures, to get a major comprehension of the radiative mechanisms linked with the atomic arrangement of molecular structures which contribute to the PL in this type of films. So, hereafter we focus specifically on the study of porous silicon which was obtained by HFCVD technique by our experimental group (unpublished results). **Figure 12** shows photoluminescence spectra between 40 and 296 K. PL measurements were carried out in vacuum and the sample was excited with a 407 nm excitation light source and an incident power of about 60 mW/mm^{-2}.

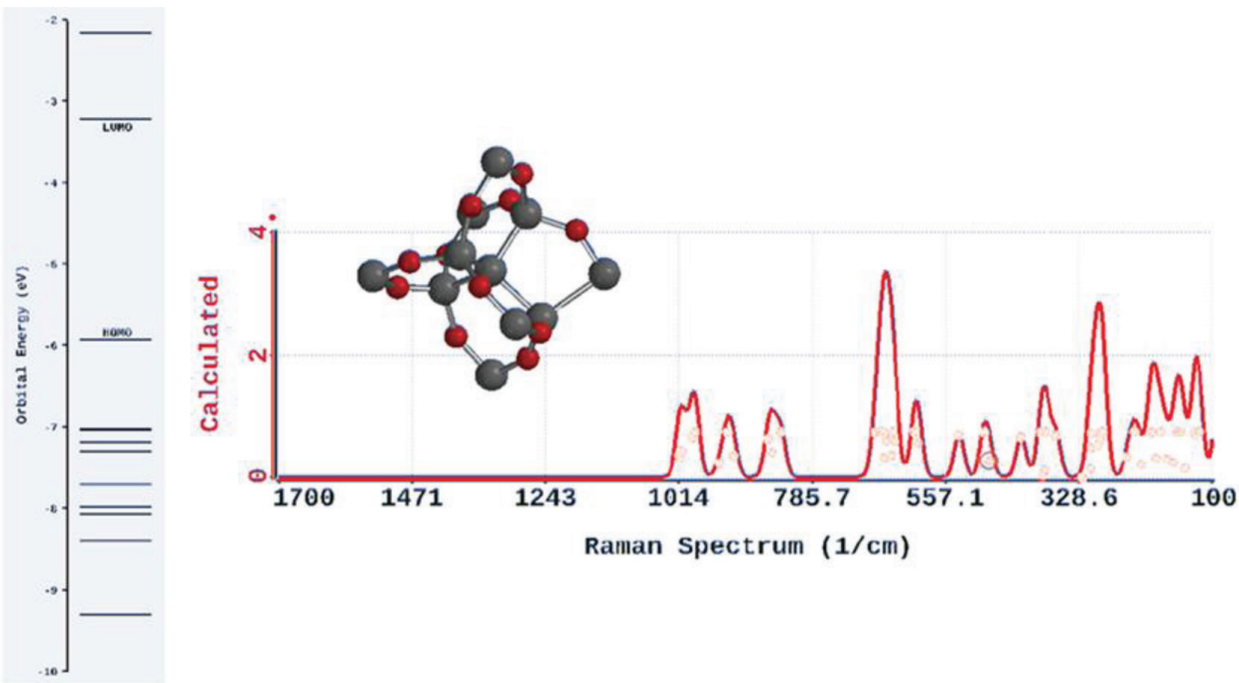

Figure 11. Theoretical Raman spectrum calculated for [$Si_{11}O_{11}$] configuration. We identify in the centre of figure the atomic structure and the left side inset displays the orbital energy in units of (eV).

http://dx.doi.org/10.5772/67614

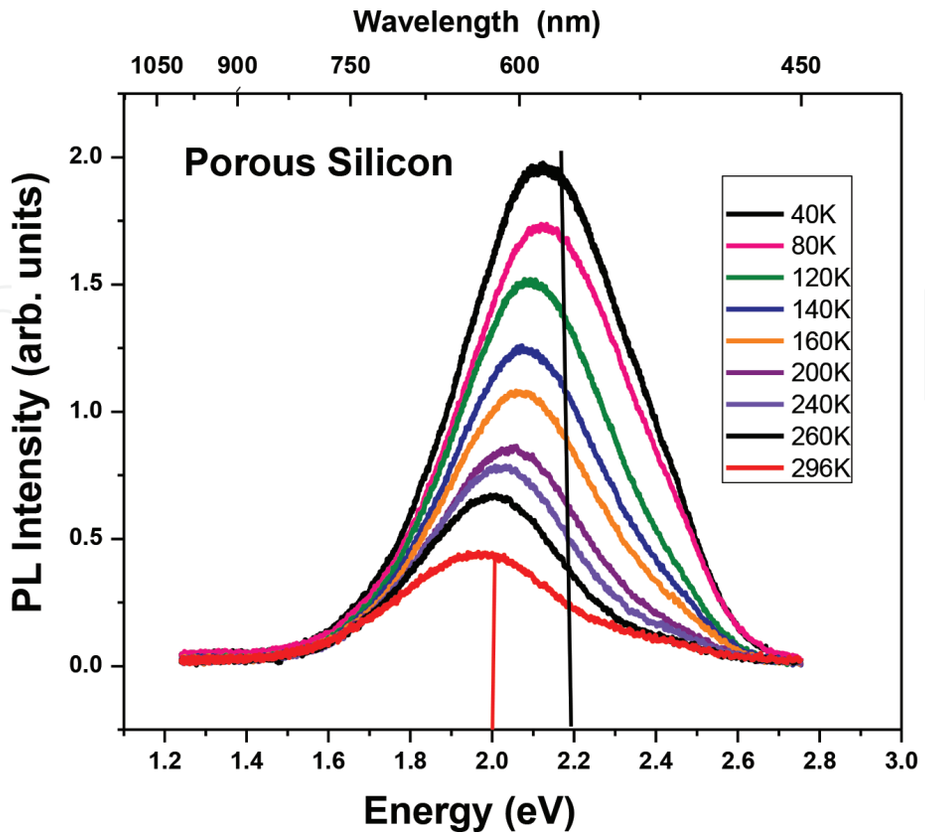

Figure 12. Experimental porous silicon PL spectra at several temperatures.

It is easily identified that the PL intensity increases as temperature decrease and at the same time the energy peak is shifted towards higher energies when decreasing the temperature of the sample. It can be seen that each peak is symmetric which means a good surface morphology and a material without defects. The shift towards higher energies is given at a rate of 5.85 E-4 eV/K. Because in our theoretical analysis neither the technique used to obtain the material nor the experimental process are relevant, since we make only use of atoms in a specific arrangement, more details about experimental conditions to grow the sample are not necessary.

In accordance with information given by PL spectra in **Figure 12**, we have that the energies of peaks of the spectra are contained approximately between 1.65 and 2.6 eV (475–750 nm). The highest intensity for each peak fit well with temperature by the following equation: $E(\text{eV}) = 2.16\,36 - 0.000585\,T(\text{K})$ for $40\,\text{K} \leq T \leq 300\,\text{K}$. Likewise, we can calculate the wavelength of the peak, if its associated energy is known, by using the simple equation $\lambda(\text{nm}) = 1240$ eV. In order to make the correlation between experimental PL results and theoretical ones, we evaluated four isomers for Si_{18} agglomerates. These correspond to isomers identified as 18A, 18B, 18C and 18D from which isomer 18D did not achieve convergence, consequently, information about it is not available. **Table 3** contains information about isomer 18A, 18B and 18C. We can appreciate that isomer 18C is not the most stable because it has the highest energy. Contrary, the isomer Si_{18A} (18A) possesses the lowest energy (a difference of 0.96 eV as indicated in third column) by this reason is the most stable of all. Other parameters of interest were calculated such as, the band gap, the dipole moment, the polarizability and the ovality.

Isomer	Energy (au)	Rel E (eV)	Band gap eV	Dipole debye	Polarizability	Wavelength nm, corresponding to highest emission intensity	Ovality
18A	–5210.83526	0.00	2.2550	2.84	75.20232	552.447567	1.25050
18B	–5210.80158	0.92	1.3883	0.04	75.20910	692.813713	1.25806
18C	–5210.80010	0.96	1.3232	0.01	75.21392	1732.74488	1.25816

Table 3. Parameters calculated for isomers Si_{18}.

With regard to Si_{18} cluster, four low-lying isomers were considered. The elongated isomer 18A has the lowest-energy at the HF/6–31G* level of theory. Moreover, the Isomer18A has its structure similar to the ground-state structure predicted by Rata et al. [35]. It contains a magic-number-cluster Si_6 unit and a hexagonal chair unit. A slight structural perturbation to this C_{3V} isomer followed by a geometry relaxation gives isomer 18B with C_S symmetry. Both 18B and 18C with C_{2V} symmetry contain tri-capped-trigonal-prism unit and are also very viable in stability compared to 18A because of the calculated difference in energy as 0.92 and 0.96 eV, respectively. Isomer 18D is a new isomer with high symmetry but relatively high energy. It is composed of two capped tetragonal anti-prisms, and we did not obtain convergence at HF/6-31G* level of theory for this isomer. We also observe from **Table 3** the predicted wavelength of the highest emission intensity corresponding to each isomer under the following order: 552.447567 nm for 18A isomer, 692.813713 nm for isomer 18B and 1732.74488 nm for isomer 18C. With this latter information we will try to make the correlation with experimental results regards PL curves shown in **Figure 12** as far as possible.

Prior to making the correlation, firstly we find out the information given in **Figure 13**, there with the naked eye, we locate at the top of the figure the FTIR spectrum and at the bottom of the one the PL spectrum both correspond to silicon agglomerate Si_{18} calculated using DFT. In the PL spectrum the appearance of the uppermost intensity peak predicted at 679.9 nm is outstanding according to our theoretical approach. Taking into account this wavelength value and making use of the simple equation to get its corresponding energy value, as just mentioned above, we obtain 1.82379 eV. This energy value when located in the experimental PL spectrum in **Figure 12** has a position as indicated by the black vertical line. As can be seen this energy may be correlated in a good approximation to the lowest PL spectrum, which corresponds to a temperature of 296 K, since it is closer to its maximum.

Evidently this theoretical energy value is shifted-left from the energy associated to the peak of more intensity of the experimental PL spectrum which is identified by the red vertical line. Although it has been possible to suggest a molecular structure in order to reproduce experimental measurements of PL spectra of porous silicon, it is obvious that our proposal may be substantially modified because of the significant discrepancies found between experimental results and theoretical predicted ones. It implies that we must reformulate our theoretical model which permits us better theoretical predictions in order to elucidate the correct molecular structure along with its composition which is responsible for radiative processes in the porous silicon; so it is a task that remains to be done. However, we may consider these results

http://dx.doi.org/10.5772/67614

as preliminary ones which can guide us along correct direction to be followed. Finally, we can see in the middle of **Figure 13** the suggested molecular structure corresponding to the isomer Si_{18}. Furthermore, the top graph in **Figure 13** represents the FTIR spectrum of the isomer 18C; it presents the two most intense peaks at the vibrational frequencies of 179 and 262 cm^{-1} where we point out that two remaining calculated wavenumbers were imaginary. The three smallest peaks appear at frequencies of 305, 390 and 434 cm^{-1}.

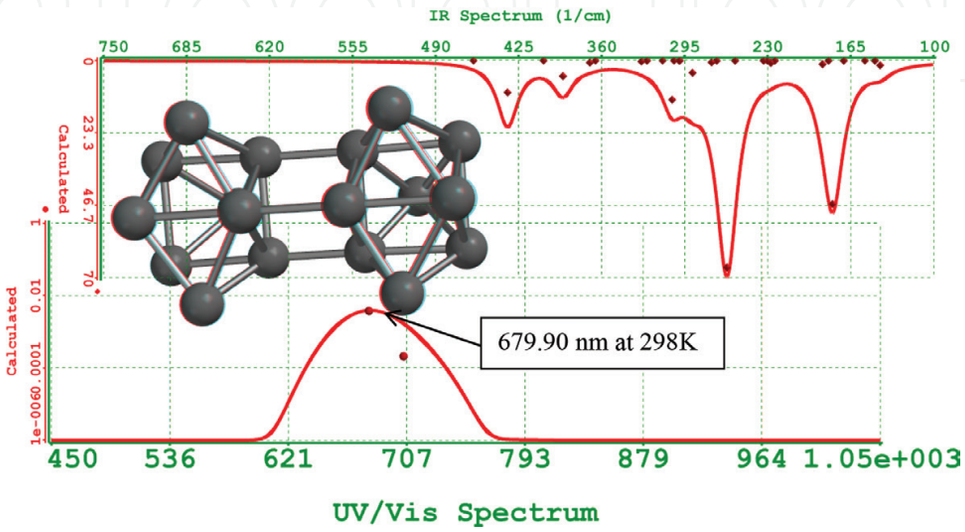

Figure 13. Top spectrum is FTIR and bottom is PL spectrum for Si_{18} C. Between graphs is represented the molecular structure.

4. Conclusions

Theoretical calculations about optical and structural properties of SiO_x films obtained experimentally by HFCVD technique have been performed using the DFT method and the GRM including temperature effects. We made correlations between theoretical results and experimental ones with respect to band gaps values, Photoluminescence and FTIR spectra. The predicted theoretical band gaps for the case of SiO_X films grown at 1300 and 1150°C are correlated with experimental values finding a good correlation since for the case of samples grown at 1300°C; it is found that E_g = 1.95 eV and the corresponding theoretical value is either E_g = 1.93 eV for a molecular structure Si_8O_8 or E_g = 1.96 eV for a molecular structure $Si_{16}O_{16}$. Likewise, for samples grown at 1150°C, E_g = 2.15 eV while theoretical results give us a value of E_g = 2.06 eV with an associated molecule type Si_9O_9. Moreover, when we correlated PL spectra with and without annealing effects, we find that a SiO_x film grown at 900°C, without annealing effects, gives a PL spectrum with two main peaks at 440 and 548 nm while theoretical spectrum shows peaks at 471and around 549.8 nm and the corresponding molecular structure is type $Si_{16}O_{16}$. In addition, the same sample with a further annealing displays luminescence peaked at 405, 749 and 820 nm and in this case theoretical results predict only one correlated peak at 415 nm using a molecule type Si_6O_6. Also, in relation to the FTIR correlation,

theoretical calculations predict frequencies of vibrational modes of bonds Si—O (rocking, bending and stretching) and Si—H (wagging, bending) whose values are well located in the experimental frequency range and the atomic structure is type $Si_{16}O_{16}$. Except for the case of the PL spectrum with annealing effects where the prediction of one peak was only possible, all theoretical predictions are well correlated with experimental measurements within experimental accuracy. Noticeable limitations in theoretical predictions are found in the case of PL porous silicon since an important difference between energies corresponding to peaks of theoretical and experimental spectra were observed, which indicates that better models must be used for this type of material.

Acknowledgements

Néstor Espinosa wants to acknowledge the support given by CONACYT (Consejo Nacional de Ciencia y Tecnología) under postdoctoral grant (reference CVU 229741).

Authors' information

Néstor David Espinosa Torres has obtained his Ph.D. at Researching Center for Semiconductors Devices (IC-CIDS) in the Science Institute from Autonomous University of Puebla, México. He worked on a theoretical study of the luminescent phenomena in silicon and silicon-rich oxide. His researching interests include modelling using molecular mechanics, semi-empirical methods, Hartree Fock and density functional theory, material science including methods for deposition and characterization techniques of semiconductors, superconductors and energy storage devices. He also has explored other topics including phtalocyanines, graphene, ZnO, TiO_2, SnO_2, MoS_2, polyoxomethalates and single and multi-wall carbon nanotubes. Currently he is a post-doctoral fellow at Instituto de Energías Renovables, UNAM campusTemixco.

José Álvaro David Hernández de la Luz is currently a researcher and professor in the Science Institute—Center of Investigation for Semiconductors Devices (IC-CIDS) from Autonomous University of Puebla, México. He has been working on optical properties of semiconductors in the framework of local and nonlocal theory, Casimir forces with dispersive spatial effects and luminescent effects in compound semiconductor. Recently, his research interest is focused on spintronics in semiconductors materials and luminescence in graphene and nanotubes of carbon.

Javier Martínez Juárez is currently a researcher and professor in the Science Institute—Center of Investigation for Semiconductors Devices (IC-CIDS) from Autonomous University of Puebla, Mexico. He has been working on families compound semiconductor III–V (GaAs, GaSb, GaAlAs, GaAlSb, GaAlSbAs, InGaSbAs), II-VI (ZnO, ZnS, CdO, CdS, CdSe, CdSSe) and IV-VI (PbS), WO_3, Cu_2O, epitaxial growth by LPE, synthesis by spray pyrolysis and chemical bath, semiconductor devices (LD and APDs), structural and photoluminescence characterization of materials and devices.

http://dx.doi.org/10.5772/67614

Author details

Néstor David Espinosa Torres[1]*, José Álvaro David Hernández de la Luz[2] and Javier Martínez Juárez[2]

*Address all correspondence to: ndet@ier.unam.mx

1 Institute of Renewable Energies (IER), National Autonomous University of Mexico (UNAM), Temixco, Morelos, Mexico

2 Researching Center for Semiconductors Devices (CIDS), Sciences Institute (ICUAP), Meritorious University Autonomous of Puebla (BUAP), Puebla, Mexico

References

[1] E. Werwa, A. A. Seraphin, L. A. Chin, C. Zhou, and K. D. Kolenbrander. Appl. Phys. Lett. 64, (1994) 1821.

[2] X. X. Wang, J. G. Zhang, L. Ding, B. W. Cheng, W. K. Ge, J. Z. Yu, and Q. M. Wang. Phys. Rev. B, 72, (2005) 195313

[3] L. T. Canham. Phys. Status Solidi B, 190, (1995) 9.

[4] G. G. Qin, and Y. J. Li. Phys. Rev. B, 68, (2003) 85309.

[5] F. G. Bell, and L. Ley. Phys. Rev. B, 37, (1988) 8383.

[6] H. R. Philipp. J. Phys. Chem. Solids, 32(8), (1971) 1935–1945.

[7] Y. N. Novikov, and V. A. Gritsenko. J. Appl. Phys., 110, (2011) 014107.

[8] D. Ristić, M. Ivanda, G. Speranza, Z. Siketić, I. Bogdanović-Radović, M. Marciuš, M. Ristić, O. Gamulin, S. Musić, K. Furić, G. C. Righini, and M. Ferrari. J. Phys. Chem. C., 116, (2012) 10039–10047.

[9] N. D. Espinosa-Torres, J. F. J Flores-Gracia, J. A. Luna-López, D. Hernández de la Luz, and J. Martí-nez-Juárez. Inte. J. Sci. Res, 3(7), (2014) 82–92 ISSN No 2277–8179.

[10] H. Wiesmann, A. K. Ghosh, T. McMahon, and M. Strongin. J. Appl. Phys., 50(5), (1979) 3752.

[11] X. QI, Z. Chen, and G. Wang. J. Mat Sci. Tech, 19(3), (1993) 235–239.

[12] M. Nayfeh, S. Rao, N. Barry, J. Therrien, G. Belomoin, A. Smith, S. Chaieb. Appl. Phys. Lett., 79, (2002) 1249–1251.

[13] L. Pavesi, L. Dal Negro, C. Mazzoleni, G. Franzo, and F. Priolo. Nature., 480, (2000) 440–444.

[14] K. Luterova, I. Pelant, I. Mikulskas, R. Tomaisiunas, D. Mueller, J.-J. Grob, J.-L. Rehspringer, and B. J. Honerlage. Appl. Phys., 91, (2002) 2896–2900.

[15] G. G. Sui, X. L. Wu, Y. Gu, and X. M. Boa. Appl. Phys. Lett., 74, (1999) 1812–1814.

[16] H. Tamura, M. Ruckschloss, T. Wirschem, and S. Veprek. Appl. Phys. Lett., 65, (1994) 1537–1539.

[17] A. J. Kenyon, P. F. Trwoga, C. W. Pitt, and G. Rehm. J. Appl. Phys., 79, (1996) 9291–9300.

[18] X. Y. Chen,Y. F. Lu,Y. H. Wu, B. J. Cho, M. H. Liu, D. Y. Dai, and W. D. Song. J. Appl. Phys., 93, (2003) 6311–6319.

[19] J. A. Luna-López, J. Carrillo-López, M. Aceves-Mijares, A. Morales-Sánchez, C. Falcony. Superficie y Vació, 21(4), (2009) 11–14.

[20] A. Barranco, F. Yubero, J. P. Espinos, F. Groening, and A. R. Gonzales-Felipe. J. Appl. Phys., 97, (2005) 113714.

[21] S. Berg, and T. Nyberg. Thin Solid Films, 476, (2005) 215–230.

[22] F. F. Gracia, M. Aceves, J. Carrillo, C. Domínguez, and C. Falcony. Superfices y Vacio, 18, (2005) 7–13.

[23] A. Benítez-Lara, G. García-Salgado, D. E. Vázquez-Valerdi, A. Morales-Sánchez, N. D. Espinosa-Torres, and J. A. Luna-López. Adv. Powder Technol., 26(1), (2015) 163–168 doi:10.1016/j.apt.2014.09.005

[24] C. Banerjee, J. Sritharathikhum, A. Yamada, and M. Konagai. J. Phys. D: Appl. Phys., 41, (2008) 185107.

[25] V. A. Gritsenko, J. B. Xu, R. W. M. Kwok, Y. H. Ng, and I. H. Wilson. Phys. Rev. Lett., 81, (1998) 1054.

[26] H. R. Philipp. J. Non-Cryst Solids., 8(10), (1972) 627–632 © North-Holland Publishing Co.

[27] J. I. Pankove. Optical Process in Semiconductors; Prentice Hall; Englewood; Cliffs; NJ; (1971) 34.

[28] J. A. Luna López, J. Carrillo López, D. E. Vázquez Valerdi, G. García Salgado, T. Díaz Becerril, A. Ponce Pedraza, and F. J. Flores Gracias. Nanoscale Res. Lett., 7, (2012) 604.

[29] Y. C. Fang, W. Q. Li, L. J. Qi, L. Y. Li, Y. Y. Zhao, Z. J. Zhang, and M. Lu. Nanotechnology., 15, (2004) 495–500.

[30] M. Aceves, A. Malik, and R. Murphy, In: Sensors and Chemometrics, eds: Maria Teresa Ramirez-Silva, (Research Signpost, ISBN: 81-7736-067-1, 2001) p.1–25.

[31] Y. Matsumoto, S. Godavarthi, M. Ortega, V. Sánchez, S. Velumani, and P. S., Mallick. Thin Solid Films., 519, (2011) 4498–4501.

[32] D. E. Vázquez-Valerdi, J. A. Luna-López, J. Carrillo-López, G. García-Salgado, A.-F. Benítez-Lara, and N. D. Espinosa-Torres, Nanoscale Res. Lett., 9 (2014) 422.

http://dx.doi.org/10.5772/67614

[33] F. Ay, and A. Aydinly,: Opt. Mater., 26, (2004) 33–46.

[34] K. Ragnar, J. A. Luna-López, O. D. Guilherme, A.-M. Mariano, and J.-B. S. Willibrordus. J. Mex. Chem. Soc., 52(3), (2008) 212–218. Sociedad Química de México. ISSN 1870-249X.

[35] I. Rata, A. A. Shvartsburg, M. Horoi, Th. Frauenheim, K. W. M. Siu, and K. A. Jackson. Phys. Rev. Lett., 85, (2000) 546.

IntechOpen

IntechOpen